Transportation Research Part D 135 (2024) 104397

Contents lists available at ScienceDirect

Transportation Research Part D

journal homepage: www.elsevier.com/locate/trd

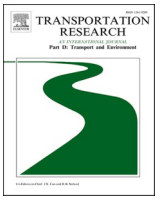

Aircraft operation reconstruction and airport noise prediction from high-resolution flight tracking data

Marco Pretto [a,*], Lorenzo Dorbolò [a], Pietro Giannattasio [a], Alessandro Zanon [b]

[a] Dipartimento Politecnico di Ingegneria e Architettura, University of Udine, Via delle Scienze 206, 33100 Udine, Italy
[b] AIT Austrian Institute of Technology GmbH, Center for Transport Technologies, Giefinggasse 2, Vienna 1210, Austria

ARTICLE INFO

Keywords:
Flight tracking
Aircraft operations
Performance modeling
Take-off weight estimation
Airport noise

ABSTRACT

Massive amounts of highly time-resolved and freely available flight tracking data are fed into a modelling tool previously devised by the authors, which was improved to perform optimal reconstruction of low-altitude aircraft operations and more accurate prediction of airport noise. The benefits of the high-resolution data, key novelty of this work, include easier flight operation identification, higher-quality ground track reconstruction, and an upgraded aircraft performance estimation. This is conducted with a new version of the authors' mixed analysis-synthesis approach, where more degrees of freedom are added to the prescribed flight procedures and the aircraft take-off weight is estimated from the tracking data. The results obtained for Zurich Airport and 2022 traffic show the ability of the proposed approach to capture the actual flight procedures during departure and arrival operations, ultimately leading to a slight underestimation (1.7 dB(A) on average) of the exposure-based cumulative noise level in the airport area.

1. Introduction

As the world is finally recovering from the COVID-19 pandemic so is doing its commercial air traffic, poised to return to 2019 figures by 2024 (IATA, 2023), while in Europe this volume should be reached by 2025 with a projected yearly growth of 1.5 % until 2029 (EUROCONTROL, 2023). This upturn is increasing again the pressure on civil airports concerning noise (ICAO, 2023), greenhouse gases, and pollutants (EUROCONTROL, 2022), to be contained with a mix of technological (Ansell, 2022) and traffic management (Degas, et al., 2022) advancements that will be applied according to their beneficial impact on the environment. This is best quantified using dedicated modelling tools (ECAC, 2016a, Filippone, 2014) such as the standard European one, EUROCONTROL's IMPACT platform (EUROCONTROL, 2024), which makes use of ECAC Doc 29 method (ECAC, 2016b) and ANP database (EUROCONTROL - ANP, 2023) to estimate near-airport aircraft performance and noise levels. However, the fidelity of its outcomes is strongly associated with the quality of the supplied air traffic data, whose provision was difficult up until recently. Instead, nowadays a powerful source is flight tracking, which relies on the ADS-B technology (Rekkas & Rees, 2008) and is based on ground receivers recording the information sent out by aircraft-mounted transponders. Many flight trackers exist currently, but the OpenSky Network (OSN) (Schäfer, et al., 2014), distinguishes itself for providing open tracking data for research purposes with time intervals as small as one second.

Within this framework, a key challenge becomes using these tracking data for the reconstruction of flight trajectories, which

* Corresponding author.
E-mail address: marco.pretto@uniud.it (M. Pretto).

https://doi.org/10.1016/j.trd.2024.104397
Received 10 May 2024; Received in revised form 24 July 2024; Accepted 29 August 2024
Available online 5 September 2024

Acronyms

ADS-B	Automatic Dependent Surveillance – Broadcast
AGL	Above Ground Level
ANP	Aircraft Noise and Performance
ARP	Airport Reference Point
ATANOMS	Airport Track and Noise Monitoring System
COVID-19	Coronavirus Disease 2019
ECAC	European Civil Aviation Conference
EU	European Union
EUROCONTROL	European Organization for the Safety of Air Navigation
FDR	Flight Data Recorder
FP	Flight Profile
GT	Ground Track
IATA	International Air Transport Association
ICAO	International Civil Aviation Organization
ISA	International Standard Atmosphere
METAR	Meteorological Aerodrome Report
MSL	Mean Sea Level
(M)TOW	(Maximum) Take-Off Weight
NPD	Noise-Power-Distance
OSN	(The) OpenSky Network
PDF	Probability Density Function
SEL	Sound Exposure Level
TMA	Terminal Manoeuvring Area

ultimately leads to the estimation of aircraft emissions. In fact, the OSN data have already enjoyed measurable success in simulating aircraft performance (Sun, et al., 2019) (Sun, et al., 2020) and at-altitude engine emissions (Filippone, et al., 2021), but many more difficulties arise when tackling the assessment of near-airport emissions. This is because the need for effective and consistent trajectory reconstruction clashes with the fact that ADS-B transmits only positional and kinematic data, often riddled also with several anomalies (Syd Ali, et al., 2016). Moreover, the emission estimation requires detailed information on both aircraft and airport areas, as well as full compatibility between emission models and trajectory reconstruction in the terminal manoeuvring area (TMA). This topic has been recently targeted by the present authors, who developed a modelling tool that makes use of ADS-B data within a modified Doc 29 method to estimate airport noise under historical (De Gennaro, et al., 2018) (Pretto, et al., 2019) and future traffic scenarios (Pretto, et al., 2020). The noise predictions were later improved by introducing a mixed analysis-synthesis approach for the aircraft performance reconstruction (Pretto, et al., 2022), according to which the prescribed Doc 29 TMA flight procedures (synthesis) were optimized in light of the flight-specific ADS-B data (analysis). However, the low ADS-B time resolution (15 s) and the unreliability of on-ground data slightly hampered the effectiveness of this approach.

Many of such limitations can be addressed by switching the data source to OSN. This gives access to much richer flight histories, which lead to more effective identification of aircraft operations in the TMA and to a better and ECAC-consistent ground track reconstruction, as recently shown by the authors (Pretto, et al., 2023). Building on this improvement, in the present work the increased data density is used to upgrade the mixed analysis-synthesis approach. This is done by reinforcing its reliance on the ADS-B data, so as to enable the synthetic ANP profiles to follow more closely the tracked aircraft trajectories. Furthermore, a solution is introduced for estimating the aircraft take-off weight (TOW) from the ADS-B initial climb speed, thus removing the need for external information on load factors, a noticeable limitation of the old mixed approach (Pretto, et al., 2022). The effects of these advancements are assessed referring to Zurich Airport, for which the results on flight operation identification, aircraft trajectory reconstruction, and noise output are presented, validated, and discussed. A solution to draw reliable yearly average contour maps based on a subset of days selected according to their weather conditions is also illustrated. The results are very promising, showing that the proposed approach can be a fully viable solution also for a longer-term objective, which is the seamless inclusion of flight tracking data into the IMPACT platform for the estimation of all types of detrimental emissions in airport areas.

The paper is structured as follows. Section 2 presents the methodological approach adopted in this work, reporting *i)* an overview of the upgraded aircraft performance and noise modelling tool, *ii)* a brief summary of new flight identification and ground track reconstruction algorithms, *iii)* a detailed presentation of the upgraded mixed approach for aircraft performance estimation and *iv)* a reminder on the noise computation method. The results are shown and discussed in Section 3 for Zurich Airport and its air traffic in 2022, while conclusions and future developments are presented in Section 4.

2. Methodology

2.1. Overview of the aircraft performance and noise modelling tool

The present aircraft performance and noise modelling tool follows the one illustrated in a previous work (Pretto, et al., 2022) but an overview is provided here also to highlight its new elements. This tool is based on the ECAC Doc 29 method (ECAC, 2016b), which enables estimation of aircraft noise through a dedicated noise computation engine, but this requires knowledge of the aircraft operations. Each operation is represented by its flight path, which is determined using synthesized procedures for the ground track (GT), the projection of the aircraft trajectory on the ground, and the flight profile (FP), which represents the aircraft motion along the ground track. All the necessary parameters are provided by the ANP database (EUROCONTROL - ANP, 2023) for about 150 reference aircraft models, known as proxies. However, the ECAC prescriptions cannot account for the large variability of real-world operations, which account for a massive number of aircraft models, evolving weather conditions, and flight plans tailored to both airport layout and aircraft payload. Instead, this variability is shown by the ADS-B data, but their straightforward use in flight mechanics equations to reconstruct the engine thrust (analytical approach) is prevented by the absence of key operational parameters such as flap settings and aircraft weight. This issue is tackled by the present tool, which combines the ECAC method with ADS-B tracking data and a number of support databases (e.g. for aircraft engines, or runway layouts) to identify actual flight operations and determine the aircraft trajectories. Flight identification and GT reconstruction are based only on the ADS-B data, while the FP computation relies on the aforementioned mixed analysis-synthesis approach. The structure of the present modelling tool is shown in Fig. 1, where three main stages can be identified:

a) pre-processing: it includes the retrieval of air traffic datasets, now conducted with the *Traffic* toolbox (Olive, 2019), and the identification of aircraft operations using some support databases;
b) processing: this consists of the GT and FP reconstruction for a given aircraft operation, from which the segmented flight path is obtained and its noise footprint is estimated;
c) post-processing: this stage includes the calculation of the cumulative noise metrics and noise contours, obtained after processing all the flight operations in a given airport and time window.

Section 2.2 illustrates only briefly data pre-processing and GT reconstruction in light of the new OSN datasets, as detailed descriptions are already available (Pretto, et al., 2023). Instead, the main contribution of this work lies in the new mixed approach for the FP reconstruction, described in Section 2.3. Finally, noise computation and post-processing stage are summarized in Section 2.4.

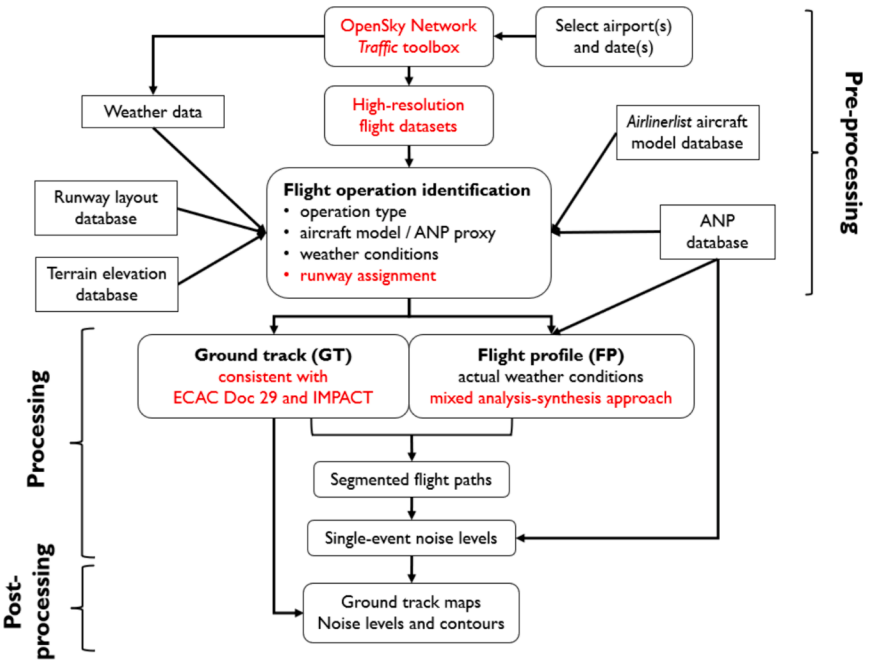

Fig. 1. Flowchart summarizing the present aircraft performance and noise modelling tool. The elements modified compared to the authors' previous work (Pretto, et al., 2022) are indicated in red. (For interpretation of the references to colour in this figure legend, the reader is referred to the web version of this article.)

2.2. Pre-processing stage and ground track reconstruction

Concerning the pre-processing stage, the main task is the collection of flight tracking data from OSN (Schäfer, et al., 2014), which is carried out by means of *Traffic* (Olive, 2019). This package allows for automatic data retrieval and dataset generation upon setting desired airport and time window, with the additional benefit of being written in *Python*, the same programming language as this modelling tool. The resulting datasets are then complemented by the weather conditions from METARs, available every 30 min and also collected using *Traffic*, and by several support databases:

- the ANP database (EUROCONTROL - ANP, 2023), together with the ANP substitution tables, which allow mapping a real-world airframe-engine combination to the ANP proxy most similar to it, also providing correction factors to account for the differences in noise output;
- the aircraft model database, which was collected from the website *Airlinerlist* (Verbrugge, 2024) and enables associating the aircraft registration number with its model, ICAO code, and age.
- the airport layout database, collected from website *OurAirports* (Megginson, 2024);
- the terrain elevation database, already in the authors' availability (Pretto, et al., 2020).

With this information in hand, the present modelling tool performs the following operations:

1) each separate flight at the selected airport is detected, assigned a unique identifier, and associated with the type of operation (departure or arrival) and its reference time (take-off or landing);
2) for each operation, the aircraft registration is used to assign the *Airlinerlist*-based aircraft model, from which ANP proxy and correction factor (number of equivalent events, N_{eq}) are retrieved;
3) the weather conditions during each operation are identified interpolating the METARs over time;
4) take-off and landing runways are assigned to each departure and arrival, respectively.

All these steps are already described in a previous work (Pretto, et al., 2022), which the reader is referred to for further details. However, for step 4) it is noted that the large amount of on-ground ADS-B information now available usually leads to a much easier, and often trivial, runway assignment (Pretto, et al., 2023). Therefore, the previous assignment strategy (Pretto, et al., 2022) is used only for the flights without on-ground data (fewer than 5 % in cases of high ADS-B coverage).

Having concluded the pre-processing, the processing of each aircraft operation can be performed. This starts from the GT reconstruction, which was previously conducted with an in-house algorithm (Pretto, et al., 2019) that fulfilled this task using only segments and circular arcs, as prescribed by ECAC. However, this algorithm did not meet the smoothness condition (i.e. heading angle continuity) required by IMPACT (EUROCONTROL, 2024), and the switch to high-resolution data prompted thorough revision of this reconstruction method. This resulted in a new algorithm, recently published and open for use by anyone (Pretto, et al., 2023), whose equations are not reported here for brevity. For the present purposes, it suffices to say that, after smoothing of the ADS-B data using a low-pass filter, the key idea is to identify the straight portions of each flight operation, to which segments with fixed heading angles are assigned. Then, between each pair of consecutive segments circular arcs are drawn that abide by the smoothness requirement, achieved by imposing tangency conditions with the existing segments and any neighbouring arcs. Finally, all arcs are sub-segmented according to the Doc 29 guidelines to enable the computation of noise levels (ECAC, 2016b). This solution was already observed to

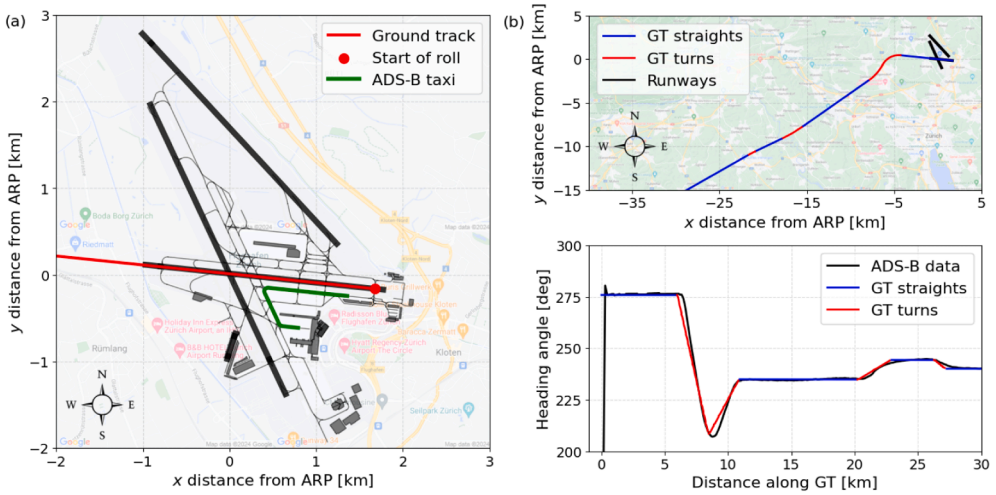

Fig. 2. (a) GT with start of roll set at the rightmost taxiway-runway crossing using ADS-B taxi positions, and (b) resulting GT with heading angle continuity ensured (departure operation at Zurich Airport).

yield satisfactory results, but in this work an additional improvement for departures was implemented that consists in using the taxi-out ADS-B data to identify the point along the runway where the aircraft starts its take-off roll. This removes the need for arbitrary placement of this point, mostly related to the unknown aircraft TOW (Pretto, et al., 2019). Examples involving the GT reconstruction are provided in Fig. 2.

2.3. Aircraft performance estimation: The mixed analysis-synthesis approach

Once the GT reconstruction has been carried out for a given flight operation, the aircraft performance estimation is conducted by determining the flight profile, which consists in the evolution of aircraft altitude, speed, and engine thrust along the curvilinear coordinate s of the GT. This is conducted with the aforementioned mixed analysis-synthesis approach, which is based on introducing, within the ANP procedures, appropriate degrees of freedom that are treated as optimization variables. Their values are then set by minimizing an objective function based on the difference between ADS-B data and ANP profile. The method builds on the authors' previous work, also retaining the expressions for pressure $p(Z)$ and temperature $T(Z)$ at altitude Z above MSL as alterations of ISA conditions (Pretto, et al., 2022). However, many improvements were introduced, and they are discussed in the following subsections. Imperial units of measurement are retained for consistency with the ANP database.

2.3.1. Mixed analysis-synthesis approach for departures

The first requirement for applying the mixed approach to departures is the calculation of the ANP synthetic flight profile, which is done using simple flight mechanics equations in conjunction with the sequence of actions (i.e. take off, climb, or accelerate) that the pilot follows when departing. However, even at fixed proxy and weight, there are up to three possible sequences (or procedures) available to the pilot, denoted as default, ICAO_A, and ICAO_B, which lead to different noise outputs and are usually associated with the noise constraints at a specific airport (ECAC, 2016a). These procedures differ mainly between 1,000 and 5,500 ft AGL, that is after the take-off roll and initial climb, but before the climb towards cruise following the switch of flap and engine settings, as shown by the example in Table 1. Moreover, the ECAC calculations always assume maximum available engine thrust and a TOW that depends only on the flight distance, reaching the maximum value (MTOW) at the largest distance. These constraints may render the synthetic profile very different from the one reported by ADS-B, but such a mismatch can be heavily reduced by loosening these constraints and allowing the synthetic profile to follow more closely the ADS-B data.

For this reason, the mixed approach requires identifying a number of optimization variables whose variation is able to provide a good degree of operational flexibility. In this work seven variables have been selected, the first four of which are the same as in the previous optimization method (Pretto, et al., 2022). These consist in the procedure type, the TOW-to-MTOW ratio denoted as K_{MTOW}, and the take-off and climb thrust reduction coefficients, K_T and K_C respectively. The latter express the fraction of maximum corrected net thrust per engine available to the aircraft $(F_n/\delta)_{max}$, which is computed using the ECAC thrust model (with $\delta = p(Z)/p_{ref}$ and $p_{ref} = 1$ atm). This computation is conducted according to Eq. (1), being K_{red} the generalized reduction coefficient and E to H the ANP thrust coefficients for either take-off or climb engine settings:

$$\left(\frac{F_n}{\delta}\right)_{red} = K_{red} \bullet \left(\frac{F_n}{\delta}\right)_{max} = K_{red} \bullet \left(E + F \bullet V_C + G_A \bullet Z + G_B \bullet Z^2 + H \bullet (T - 273.15)\right) \tag{1}$$

However, three new variables have been added to enhance the flexibility within a given procedure: Δh_L, Δh_M and f_e. In particular, Δh_L

Table 1
Default (top) and ICAO_A (bottom) procedural steps for an A320-211 departing at minimum ANP weight.

Step nr	*Step*	*Flap settings*	*Engine settings*	*Height AGL h [ft]*	*Calibrated airspeed V_C [kt]*	*Climb rate[ft/min]*	*Energy share [%]*
1	*Take off*	1 + F	MaxTakeoff	–	–	–	–
	Take off	1 + F	MaxTakeoff	–	–	–	–
2	*Climb*	1 + F	MaxTakeoff	1,000	–	–	–
	Climb	1 + F	MaxTakeoff	1,500	–	–	–
3	*Accelerate*	1 + F	MaxTakeoff	–	186.2	1150.5	69.1
	Climb	1 + F	MaxClimb	3,000	–	–	–
4	*Accelerate*	1	MaxTakeoff	–	208.1	1300.7	69.8
	Accelerate	1 + F	MaxClimb	–	186.1	812.1	69.6
5	*Climb*	ZERO	MaxClimb	3,000	–	–	–
	Accelerate	1	MaxClimb	–	201.2	933.5	70.6
6	*Accelerate*	ZERO	MaxClimb	–	250.0	1230.7	69.0
	Accelerate	ZERO	MaxClimb	–	228.2	1119.7	69.9
7	*Climb*	ZERO	MaxClimb	5,500	–	–	–
	Accelerate	ZERO	MaxClimb	–	250.0	1240.5	69.6
8	*Climb*	ZERO	MaxClimb	7,500	–	–	–
	Climb	ZERO	MaxClimb	5,500	–	–	–
9	*Climb*	ZERO	MaxClimb	10,000	–	–	–
	Climb	ZERO	MaxClimb	7,500	–	–	–
10	*Climb*	ZERO	MaxClimb	10,000	–	–	–

and Δh_M are added to the initial (after taking off, before the first 'accelerate' step) and mid-climb (below 5,500 ft) steps respectively, while f_e is multiplied to each energy share, which is the percentage of engine thrust dedicated to accelerating the aircraft, while the remainder is used for climbing. Table 2 reports their ranges, also including the additional constraints applied to prevent calculation of unrealistic profiles for some proxy-profile pairs. Furthermore, now K_C is decoupled from K_T, and, while $K_{MTOW,min}$ is computed as in the previous work assuming 20 % payload and minimum fuel to complete the flight, its upper bound is always 1.

Having set the variables, the mixed approach proceeds by minimizing an objective function, *OBF*, which is composed of a measure of the distance between ADS-B data and synthetic profile, RMS_{ZV}, and a correction factor, *CF*, that acts as a penalty function, as illustrated in Eq. (2):

$$OBF = RMS_{ZV} + CF. \tag{2}$$

Both these components need to be defined, and their definitions differ from those in the authors' previous work (Pretto, et al., 2022). Firstly, RMS_{ZV} is computed as shown by Eqs. (3a) to (3c),

$$\begin{cases} RMS_{ZV} = RMS_Z + 25 \bullet RMS_V, & (3a) \\ RMS_Z = 20\sqrt{\frac{1}{N_L}\sum_{i=1}^{N_L}\left(Z_{FP,i} - Z_{ADSB,i}\right)^2} + 10\sqrt{\frac{1}{N_M}\sum_{i=1}^{N_M}\left(Z_{FP,i} - Z_{ADSB,i}\right)^2} + \sqrt{\frac{1}{N_H}\sum_{i=1}^{N_H}\left(Z_{FP,i} - Z_{ADSB,i}\right)^2}, & (3b) \\ RMS_V = 20\sqrt{\frac{1}{N_L}\sum_{i=1}^{N_L}\left(V_{FP,i} - V_{ADSB,i}\right)^2} + 10\sqrt{\frac{1}{N_M}\sum_{i=1}^{N_M}\left(V_{FP,i} - V_{ADSB,i}\right)^2} + \sqrt{\frac{1}{N_H}\sum_{i=1}^{N_H}\left(V_{FP,i} - V_{ADSB,i}\right)^2}, & (3c) \end{cases}$$

where *Z* and *V* denote altitude [ft] and ground speed [kt] respectively, while subscript *FP* indicates the profile synthesized according to the optimization variables and *ADSB* the recorded *i*-th data point at same GT coordinate s_i. Coefficient 25 ft/kt is used in RMS_{ZV} to weigh the speed component, RMS_V, against the altitude one, RMS_Z. This choice was made after careful analysis of ADS-B profiles and their impact on aircraft noise, and implies that a 1-knot error in the aircraft speed has the same impact as a 25-foot error in its altitude. This value is sensible considering the heights and speeds of typical departure manoeuvres, allowing in particular easier discrimination between 'climb' and 'accelerate' steps during the optimization (see Table 1). Moreover, each *RMS* is split into three components, which are the low-, mid-, and high-height ones, with each component having respectively subscripts L, M, H. The low-height component includes all N_L points below 1,500 ft AGL, the mid-height one all N_M points between 1,500 ft and 5,000 ft AGL, and the high-height one all N_H points above 5,000 ft. A weighting coefficient of 20 is applied to the low-height component to give the most relevance to the take-off roll and initial climb, which are the noisiest departure phases (ECAC, 2016a) and thus demand the highest reconstruction accuracy. Then, the mid-height coefficient (10) is large enough to allow the mixed approach to detect the departure procedure used by the pilot, while the last coefficient (1) is kept low since that portion of the climb affects noise levels and procedure detection the least. The three weighting coefficients were selected following the analysis of several hundred flight operations performed by small and large aircraft of all major manufacturers at multiple airports.

With RMS_{ZV} defined, the focus is now placed on correction factor *CF* in Eq. (2), whose role is to address some key issues of an insufficiently constrained optimization procedure. Primarily, these are the lack of tracking-based information on the aircraft TOW, and the reliance on a flight mechanics computation whose output depends mostly on the ratio between corrected net thrust per engine, F_n/δ, and TOW rather than on their separate values (ECAC, 2016b). Leaving these elements unaddressed may lead to peculiar results, among which two are of high relevance:

1) very low TOW coupled with very low thrust;
2) very high TOW coupled with very low thrust.

However, analysis of FDR data from many aircraft and several aircraft models (Koudis, et al., 2017) show that both of these cases are very unlikely. For case 1), the reason is that aircraft tend to fly with as much payload (passengers or cargo) as possible, thus minimizing the chance of a low TOW. Additionally, heavy aircraft depart with high thrust to keep the take-off roll distance contained within the limits of runway length and associated safety margins, which makes case 2) a rare occurrence.

This issue is addressed in two steps. Firstly, the ECAC-based Eq. (4) is used to estimate the TOW, exploiting its relationship with take-off calibrated airspeed V_{CTO} through ANP-based lift coefficient *C*. This can be done because V_{CTO} can be extracted from the ADS-B

Table 2
Optimization variables of the mixed analysis-synthesis approach for departures.

Variable	Symbol	Type	Values/ranges	Purpose
Procedure type	P_{type}	Discrete	Default/ICAO_A/ICAO_B	Procedural flexibility
Take-off thrust reduction	K_T	Continuous	[0.75, 1]	Variable take-off thrust
Climb thrust reduction	K_C	Discrete	1.0/0.9/0.8	Variable climb thrust
Weight fraction	K_{MTOW}	Continuous	[$K_{MTOW,min}$, 1]	Variable weight
Initial climb height	Δh_L	Continuous	[-2000 ft, 500 ft], as long as $h_{initial\ climb} > 800$ ft	Flexible initial climb step(s)
Mid-climb height	Δh_M	Continuous	[0 ft, 3000 ft], as long as $h_{mid-climb} < 5{,}500$ ft	Flexible mid-climb step(s)
Energy share fraction	f_e	Continuous	[0.7, 1.4], as long as energy share < 100 %	Flexible acceleration step(s)

lift-off speed, now identifiable from the high-resolution OSN data. This yields an estimate for K_{MTOW}, denoted as $K_{MTOW,est}$.

$$V_{CTO} = C\sqrt{TOW}. \tag{4}$$

The second step is using this value in the correction factor. This is done defining CF as per Eq. (5):

$$CF = RMS_{ZV}\left[max(0, K_{MTOW} - K_T) + \left(exp(\left|K_{MTOW,est} - K_{MTOW}\right|) - 1\right)\right], \tag{5}$$

which acts as a two-pronged penalty function that multiplies the calculated RMS_{ZV}. The first part of the penalty is linear and is applied when $K_{MTOW} > K_T$, with the main goal of preventing case 2) above. Instead, the second part acts when K_{MTOW} differs from $K_{MTOW,est}$, but it is applied as a symmetrical exponential penalty that becomes particularly relevant only when $\left|K_{MTOW} - K_{MTOW,est}\right| > 0.05$. The reasons are a certain and unavoidable unreliability of the ADS-B data, and the fact that the actual take-off speed can be up to a few knots higher than the V_{CTO} from Eq. (4) (ECAC, 2016b). These elements contribute to making $K_{MTOW,est}$ just a reference rather than a certainty, especially if the remainder of the profile gives better results with $K_{MTOW} \neq K_{MTOW,est}$. Note that this solution is a major improvement compared to the previous work (Pretto, et al., 2022): the reliance on external historical information, such as the load factor distributions previously used to predict present and future K_{MTOW} frequencies, has been completely removed, and the departure optimization now depends only on the ADS-B information referring to that specific flight.

Finally, the minimization of the objective function is conducted by means of a basin-hopping algorithm (Wales & Doye, 1997), which enables more effective identification of the global minimum in problems with multiple local minima such as this one, dominated by the thrust-to-weight ratio.

The mixed approach as illustrated here is applied to all pre-processed departure operations, and it leads to very good results in the vast majority of cases, that is when the ADS-B-derived profiles are at least somewhat similar to the ANP procedures. However, if the departure procedure is not covered by ANP, which is more likely to happen with small aircraft, the mixed approach provides only minor improvements. Examples of these opposite occurrences are provided in Fig. 3.

2.3.2. Mixed analysis-synthesis approach for arrivals

The mixed approach for arrivals is much simpler than that for departures, primarily because of the much higher degree of prescription in the ECAC calculations. In particular, for each ANP proxy the landing weight is fixed, only a default profile is available, all descent angles are imposed rather than computed from energy shares or vertical rates, and the thrust outputs are mainly inferred from aerodynamic and kinematic quantities. Despite these constraints, during the final descent (below 1,500 ft AGL) the ANP profiles match quite well the ADS-B data, while more variability appears to be required above it. This aligns with the observations of the previous work (Pretto, et al., 2022), and the optimization procedure is conducted accordingly. Firstly, the optimization variables and their ranges are the same as in the previous work, as listed in Table 3, the only exceptions being the height and length intervals of the level-flight phase, extended after analysis of many ADS-B datasets.

Then, the optimization is conducted by minimizing the OBF of Eq. (2) with RMS_{ZV} computed for all N points via Eq. (6), that is without height components, not very useful due to the many constraints:

$$RMS_{ZV} = RMS_Z + 25 \bullet RMS_V = \sqrt{\frac{1}{N}\sum_{i=1}^{N}\left(Z_{FP,i} - Z_{ADSB,i}\right)^2} + 25\sqrt{\frac{1}{N}\sum_{i=1}^{N}\left(V_{FP,i} - V_{ADSB,i}\right)^2}. \tag{6}$$

Moreover, $CF = 0$ since no penalty is justified when the landing weight is fixed and, more importantly, impossible to infer from the

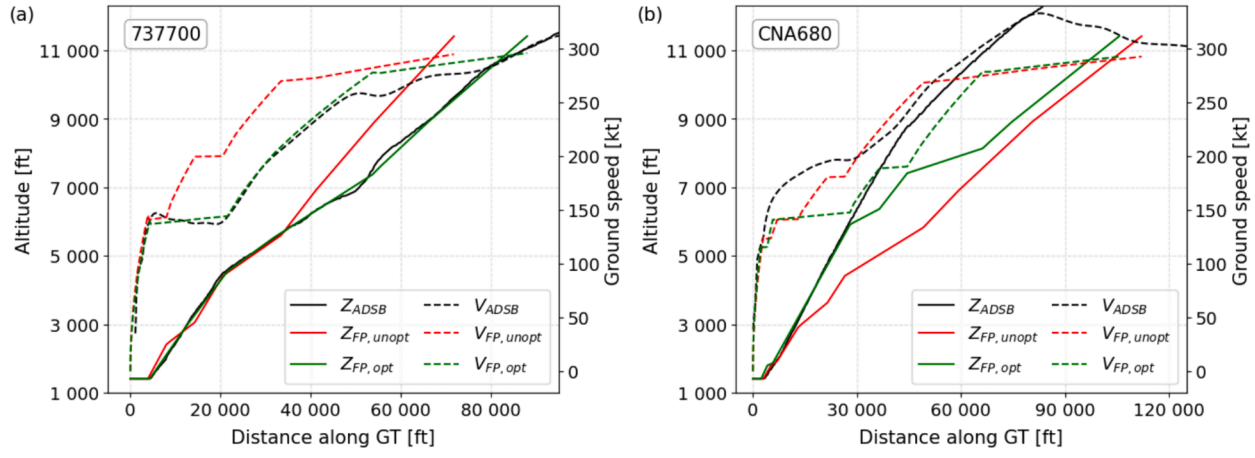

Fig. 3. At Zurich Airport, (a) optimized departure FP when ADS-B data are similar to a procedure (here ICAO_A) covered by ANP, and (b) optimized departure FP in the case of a procedure outside the ANP coverage.

Table 3
Optimization variables of the mixed analysis-synthesis approach for arrivals.

Variable	Symbol	Type	Values/ranges
Initial descent angle	γ_{in}	Continuous	[1.5 deg, 5 deg]
Initial descent calibrated airspeed	$V_{C,in}$	Continuous	[200 kt, 250 kt]
Length of level-flight phase	Δs_{lev}	Continuous (if present)	[40 %, 250 %] of ANP length, or removed
Height of level-flight phase	h_{lev}	Continuous (if present)	[1,500 ft, 4,500 ft] AGL, if level is present

ADS-B data. In addition to the use of a basin-hopping minimization algorithm, the other novelty worth mentioning for the present approach is represented by the level-flight phase. In fact, in addition to removing this phase if the ADS-B data suggest its absence, thus covering the possibility of capturing even a continuous descent operation, such a phase is added to each ANP profile and applied to the operation if it leads to a better match with the ADS-B profile. The added level phase varies according to Table 3.

The mixed approach as illustrated is applied to all pre-processed arrival operations, and similarly to its departure counterpart it yields satisfying results in the majority of cases, particularly when the ADS-B profiles are reasonably close to the pre-existing ANP procedures. However, problems arise if the actual approach procedure is not covered by ANP: this time it can happen also to larger aircraft, but the detrimental effects seem contained since the aircraft has to land, and the final approach is always conducted at about 3 deg and 100 to 150 kt, depending mostly on the aircraft size (ECAC, 2016b). Relevant examples referring to these opposite cases are provided in Fig. 4.

2.4. Noise calculation: Single-event and cumulative noise levels

For a single flight operation, the GT and FP obtained as illustrated in the previous sections are merged to generate the segmented flight path without any difference compared to the original formulation (Pretto, et al., 2019). This enables calculation of the A-weighted sound exposure level (SEL) L_{AE} and maximum sound level L_{Amax}, which is carried out using the ECAC Doc 29 noise computation engine and a 2D matrix of sound receivers, or observers, that cover the airport area, including also their elevation as available from terrain relief maps (Pretto, et al., 2020). At fixed observer, each j-th path segment is treated as an independent noise event that generates $L_{AE,j}$ and $L_{Amax,j}$, which are obtained by modifying the NPD baseline levels provided by ANP according to corrected net thrust, observer-segment distance, and several adjustment terms that depend on aircraft speed, engine placement, observer-segment view angle, and segment length. Weather conditions and line-of-sight blockage are considered as well. Finally, the effects of all N path segments are cumulated for each observer according to Eq. (7), which yields the single-event noise levels:

$$\begin{cases} L_{AE} = 10 \bullet \log_{10}\left(\sum_{j=1}^{N} 10^{\frac{L_{AE,j}}{10}}\right) + 10 \bullet \log_{10} N_{eq}, \\ L_{Amax} = \max\left(L_{Amax,i}\right) + 10 \bullet \log_{10} N_{eq}. \end{cases} \tag{7}$$

The computation is performed for all flight operations around an airport and within a set time window, assuming each operation to correspond to a sound event. Single-event levels are then used to compute time-weighted equivalent sound levels, which account for the overall acoustic energy from multiple events over a set time period. Eq. (8) reports the general expression for time-weighted levels $L_{Aeq,W}$:

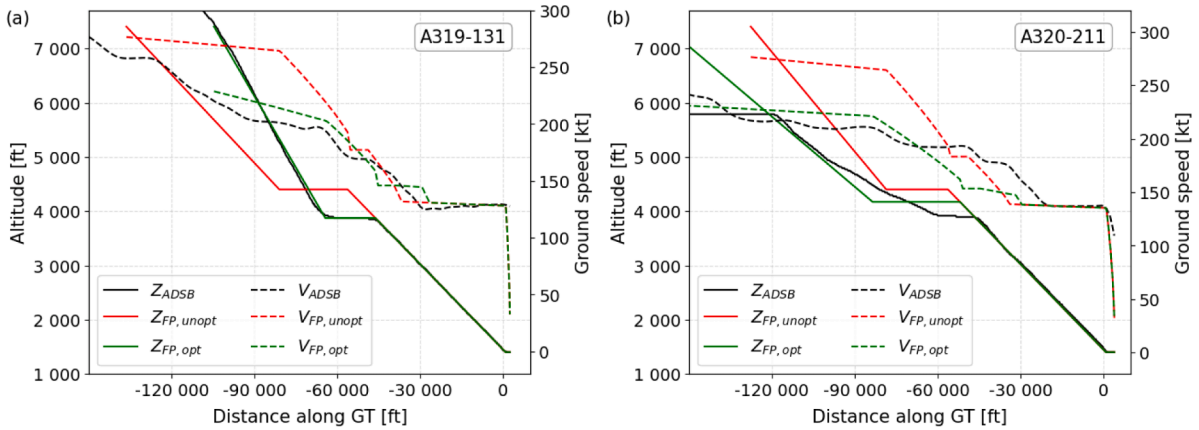

Fig. 4. At Zurich Airport, (a) optimized arrival FP when ADS-B data are similar to a procedure covered by ANP, and (b) optimized arrival FP in the case of a procedure outside the ANP coverage.

$$L_{Aeq,W} = 10 \bullet \log_{10}\left(\frac{t_0}{T} \bullet \sum_{i=1}^{M} g_j \bullet 10^{\frac{L_{AE,i}}{10}}\right), \tag{8}$$

where $L_{AE,i}$ is the single-event SEL, $t_0 = 1\ s$ due to the A-weighting, and M is the number of noise events considered during time period T, with g_j being a time-of-day dependent factor. Different metrics correspond to specific values of T and g_j, which are reported in Table 4. These equivalent levels are then used to draw, by means of a 'marching squares' algorithm, the noise contour maps, which are superimposed onto a satellite map of the airport area. Similar operations can be conducted for maximum-level indices, but they are not used in this work. More details are found in the authors' previous contributions (Pretto, et al., 2019) (Pretto, et al., 2022).

3. Results

The airport selected for the present work is Zurich Airport, located 13 km to the North of Zurich and accounting for three runways, almost 600 daily flight operations, and around 30 million passengers per non-COVID year (Flughafen Zürich, 2024a). The selection was made because large amounts of historical information are available on daily air traffic volume and noise levels, including both contour maps and measurements, on which consolidated results are provided for 2022. Section 3.1 first explains how a representative set of air traffic days at the airport was selected, and then discusses the resulting ground tracks, including also the validation of the GT reconstruction algorithm. Section 3.2 tackles the analysis of the flight profiles resulting from the application of the upgraded mixed analysis-synthesis approach, providing separate examination of departures and arrivals. Finally, Section 3.3 discusses the airport noise results, focusing on the comparison of the present noise predictions with official noise contours and actual measurements taken at the monitoring stations.

3.1. Chosen air traffic days, traffic coverage, and ground track reconstruction

For a full reconstruction of yearly average noise levels around an airport it would be necessary to collect and process the traffic data of every day of the year, which, while technically feasible, would demand significant computational capabilities. Instead, a more viable strategy, already adopted by the authors in a previous work (Pretto, et al., 2019), is to select a small sample of days in which flight operations and weather conditions are representative of the average air traffic in the year. This may be very difficult to do for each airport worldwide, but in the present work a general-purpose solution is proposed and applied to Zurich Airport. This solution involves selecting traffic days where *i)* the daily traffic coverage is as close to 100 % as possible, and *ii)* the cumulated daily weather conditions are representative of the yearly ones. The selection was conducted using daily flight tables and METARs downloaded from OSN, among which 23 days were chosen as a representative sample of the entire 2022. For requirement *i)*, the OSN operations were compared with the traffic data provided by the airport (Flughafen Zürich, 2024b), and Fig. 5(a) shows a good result for all 23 days, with a mean coverage of 96.7 %. For requirement ii), while the 23 days were selected to span all four seasons, the key factor that was considered is the wind direction, as it affects massively the low-altitude flight operations, and hence the noise footprints. The distribution of wind directions from the METARs for the entire 2022 was compared to that of the 23 days selected, with the results shown in the wind rose of Fig. 5(b). This comparison is successful, indicating that this 23-day set can be considered a good proxy for the yearly airport traffic, and the present tool was applied to this set to estimate TMA aircraft performance and airport noise.

The first result from the modelling tool consists in the reconstructed ground tracks, which are reported in the GT map of Fig. 6(a). The map shows that the preferential TMA directions are NW and W, although a large number of arrivals took place also on runway 14 (SE direction), but also that all runways were used, mainly depending on the daily wind direction. Unsurprisingly, along the runway directions are located the 14 ATANOMS monitoring stations (Flughafen Zürich, 2023), which keep track of noise levels linking the measurements to radar data and flight plans from the airport authority. Runways and locations of ATANOMS stations are shown in Fig. 6(b).

Then, the validation of the GT reconstruction algorithm is conducted by examining the projection errors between ground tracks and ADS-B positions, with each error defined as the distance between ADS-B point before low-pass filtering and corresponding GT segment. The errors were computed for all ADS-B points of all operations, thus leading to several error-related PDFs. Firstly, Fig. 7(a) reports in a semi-logarithmic scale the global PDF of all GT errors, as well as the separate PDFs hosting the errors related only to straight segments and turns respectively, with their median values also added as dashed lines. The global median error is 15 m, and the number of points with error under 100 m is 86 %, which can be considered satisfying considering the presence of noise in the ADS-B data, which required

Table 4
Cumulative noise indices for A-weighted sound exposure levels.

Name	$L_{Aeq,W}$	T [s]	g_j		
			day	evening	night
24-hour average sound level	$L_{Aeq,24h}$	86,400	1	1	1
16-hour day average sound level	$L_{Aeq,day}$	57,600	1	1	0
8-hour night average sound level	$L_{Aeq,night}$	28,800	0	0	1
Day-night average sound level	L_{DN}	86,400	1	1	10
Day-evening-night average sound level	L_{DEN}	86,400	1	$\sqrt{10}$	10

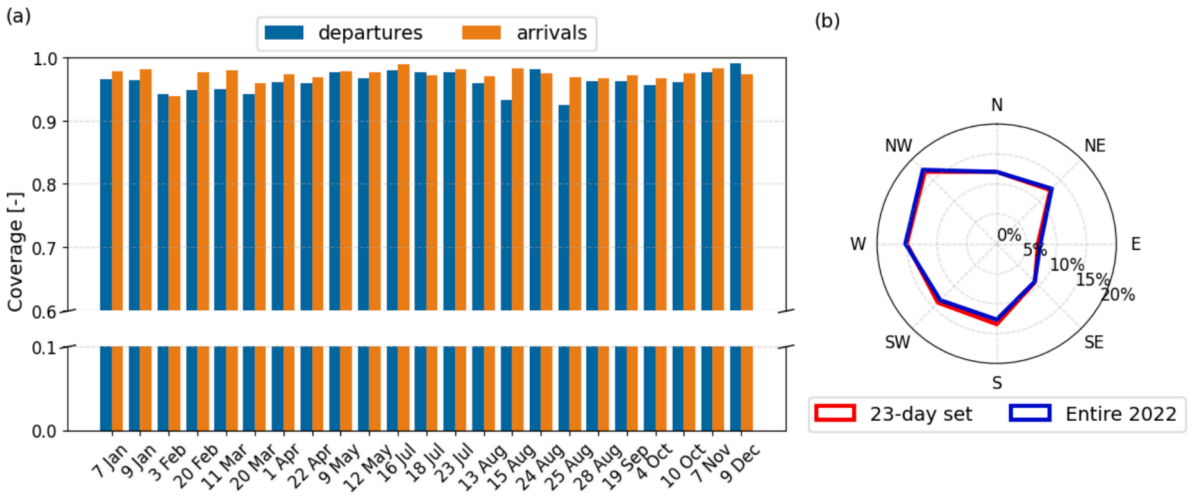

Fig. 5. (a) OSN traffic coverage of the 23 days (mean coverage: 96.7 %), and (b) distribution of wind directions.

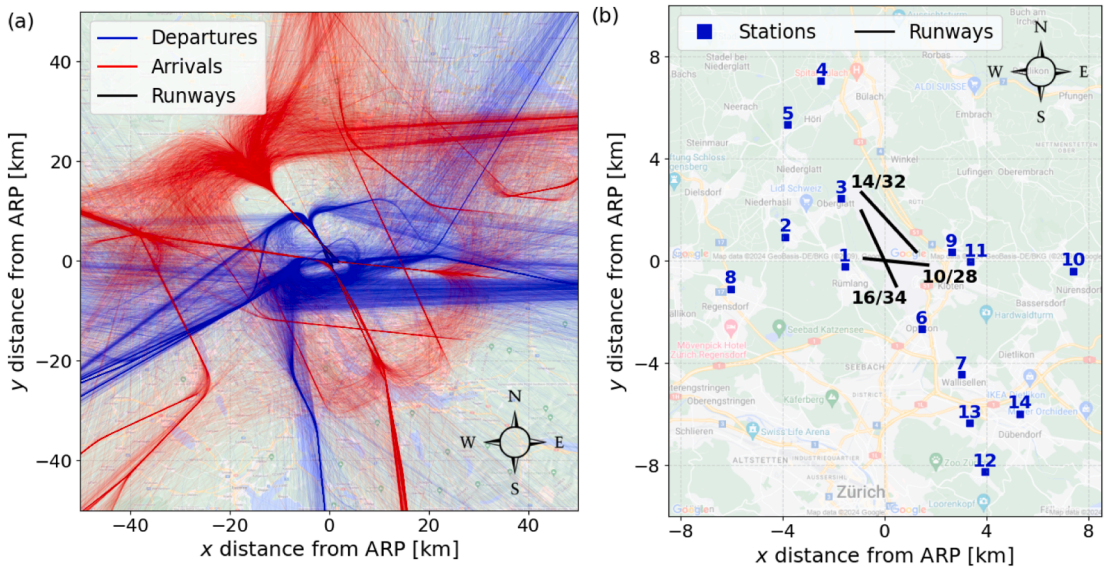

Fig. 6. (a) Ground track map of air traffic around Zurich Airport including all 23 days selected, and (b) airport runways and ATANOMS monitoring stations.

low-pass filtering. Furthermore, the median error for turns is just moderately higher than the one for straight segments (23 m vs 13 m), suggesting that aircraft turns can be modelled quite well using only circular arcs. The only downside is the 2 % of points with errors over 500 m, an examination of which is conducted in Fig. 7(b) with a dedicated PDF. Analysis of this PDF indicates that the vast majority of such errors occurred more than 20 km away from the airport, with the root cause being the Cartesian-geographic coordinate conversion, unsuited at large distances from the airport. All these findings are consistent with those of the previous work (Pretto, et al., 2023) despite the different airport and a larger flight dataset, confirming the reliability of the present GT reconstruction algorithm when focus is put on the aircraft operations in the TMA.

3.2. Reconstruction of the flight profiles with the upgraded mixed analysis-synthesis approach

The section is dedicated to the results obtained with the application of the upgraded mixed analysis-synthesis approach. The departures are discussed in Section 3.2.1, while the arrivals in Section 3.2.2.

3.2.1. Mixed approach applied to the departure flight profiles

A quantification of the improvements obtained with the upgraded mixed approach applied to departures compared to the baseline

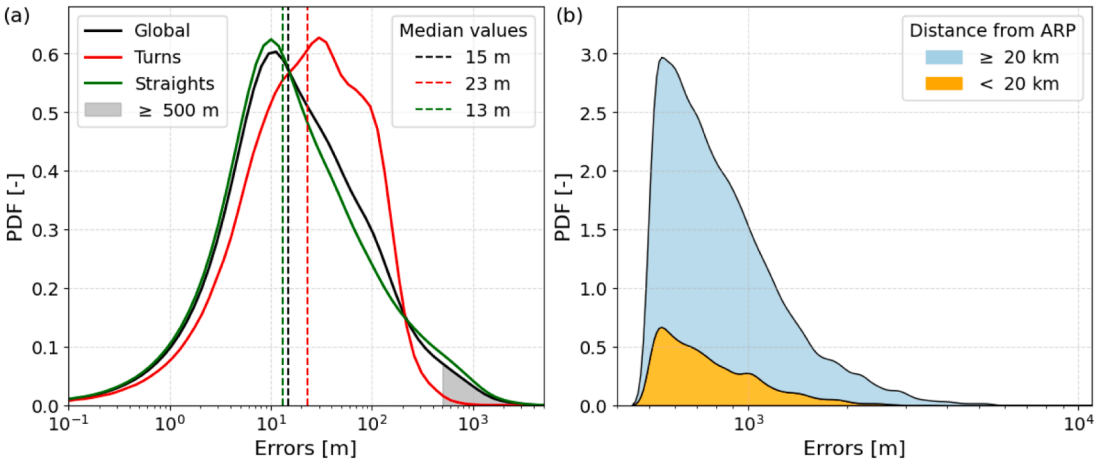

Fig. 7. (a) PDFs of GT errors accounting for all ADS-B points and separately for straight-flight segments and turns, and (b) PDFs of GT errors focusing on those over 500 m.

ECAC method is provided in Fig. 8. Firstly, Fig. 8(a) illustrates the statistical distribution, along with its mean and median, of the ratio between optimized and non-optimized RMS_{ZV} for all the departures, with non-optimized value $RMS_{ZV,unopt}$ computed using the default ANP procedures with maximum available thrust ($K_{red} = 1$) and flight-distance-dependent TOW as suggested by ECAC. The distribution median is 0.41, meaning that the overall RMS_{ZV} reduction is close to 60 %, a promising result considering that key elements such as ANP step sequences and flap settings were preserved. Moreover, around 99 % of departures experience a measurable reduction in RMS_{ZV}, while the remaining 1 % with RMS_{ZV} ratio near 1 is performed by very small aircraft with poor ANP procedures. This consideration is strongly supported by the results in Fig. 8(b), which shows the impact of the optimization expressed through medians and confidence intervals of the RMS_{ZV} ratio separately for each proxy, whose name is listed on the x-axis.

This figure highlights that the proxies representing the most common aircraft (i.e. recent Airbus, Boeing, and Embraer models) have better outcomes compared to the ones mapped to smaller aircraft and private jets. The Boeing 767–300 is the only exception, but it is simply due to its age (over 40 years), which results in ANP lacking the procedural flexibility added to more recent proxies.

In the case of departures, the validity of the mixed approach is further confirmed by two additional considerations. The first one relates to the departure procedure: since basically all flights leaving Zurich Airport follow ICAO_A procedures (Schwab & Zellmann, 2020), it is expected that the present tool be able to recognize this profile type. Indeed, this is confirmed by Fig. 9(a), where about 85 % of all departures are correctly classified as following ICAO_A profiles. However, if this analysis is repeated removing the older or smaller ANP proxies that have only default profiles (i.e. no ICAO step sequences), the frequency of ICAO_A profiles rises to 97.9 %, which is very close to 100 % and fully consistent with the referenced literature source.

The second consideration regards the thrust-weight relationship, which consists in the behaviour of thrust reduction K_{red}(both K_T and K_C) compared to the TOW ratio, K_{MTOW}. This is shown for all departures in the scatter plot of Fig. 9(b), together with the PDFs of K_{MTOW} and K_T, respectively plotted along the x- and y-axes. Firstly, and most importantly, this scatter plot has a very similar appearance to those from literature (Koudis, et al., 2017): there is a clearly visible diagonal, where $K_T \cong K_{MTOW}$, the vast majority of departures are placed to the left of it, where $K_T > K_{MTOW}$, and two accumulations are observed at $K_T \cong 1$ (larger) and $K_T \cong 0.75$

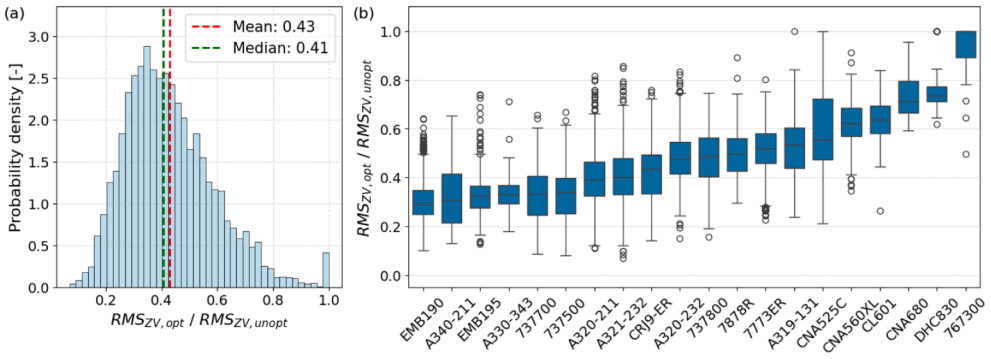

Fig. 8. (a) distribution of RMS_{ZV} ratio considering all departures, and (b) RMS_{ZV} ratio for each ANP proxy ordered by median, with blue bars and black lines denoting confidence intervals of 50 % and 95 %, respectively (empty circles = outliers beyond 95 % confidence). (For interpretation of the references to colour in this figure legend, the reader is referred to the web version of this article.)

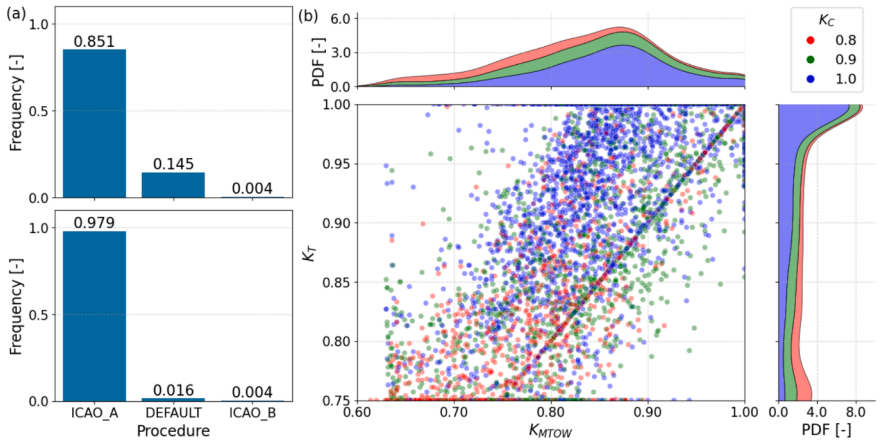

Fig. 9. (a) departure procedure identification results upon application of the mixed approach before (top) and after (bottom) removing the default-only ANP proxies, and (b) $K_T - K_C - K_{MTOW}$ relationship, expressed as a scatter plot accompanied by PDFs of K_T and K_{MTOW} on the appropriate axes.

(smaller). Furthermore, high K_C values are mostly associated with high K_T and K_{MTOW}, whereas low K_C with similarly low K_T and K_{MTOW}. Secondly, although this good result was partly prompted by the correction of Eq. (5), the only 'external' penalty was the one that keeps the likelihood of $K_{MTOW} > K_T$ cases low. This occurrence, particularly true in actual departures, was impossible to replicate without a penalty due to the limitations of the ANP database (e.g. lack of ICAO profiles for some proxies). However, the penalty is weaker near the $K_T = K_{MTOW}$ diagonal, which let around 5 % of departures fall to the right of it. Such a small value is reasonable and consistent with the literature, and it contributes to making the overall modelled thrust-weight relationship quite satisfying.

Finally, the importance of selecting an appropriate thrust-weight combination is examined in terms of noise output. This is done with the example in Fig. 10, which presents the effects of two different thrust-weight pairs for a straight-line ICAO_A departure of a 737 MAX 8 at ISA conditions. Two cases are examined: a low-weight departure, with $K_{MTOW} = 0.85$, $K_T = K_C = 0.8$, and a max-weight (MTOW) one, with $K_{MTOW} = K_T = K_C = 1$. The figure shows clearly the similarities between the two kinematic profiles, with almost equal altitudes and marginally different (10 to 15 knots) ground speeds. However, the MTOW case has up to 25 % higher thrust, which results in a much wider noise footprint, with SEL values that, apart from the small area beneath the aircraft, can be up to 3 dB(A)

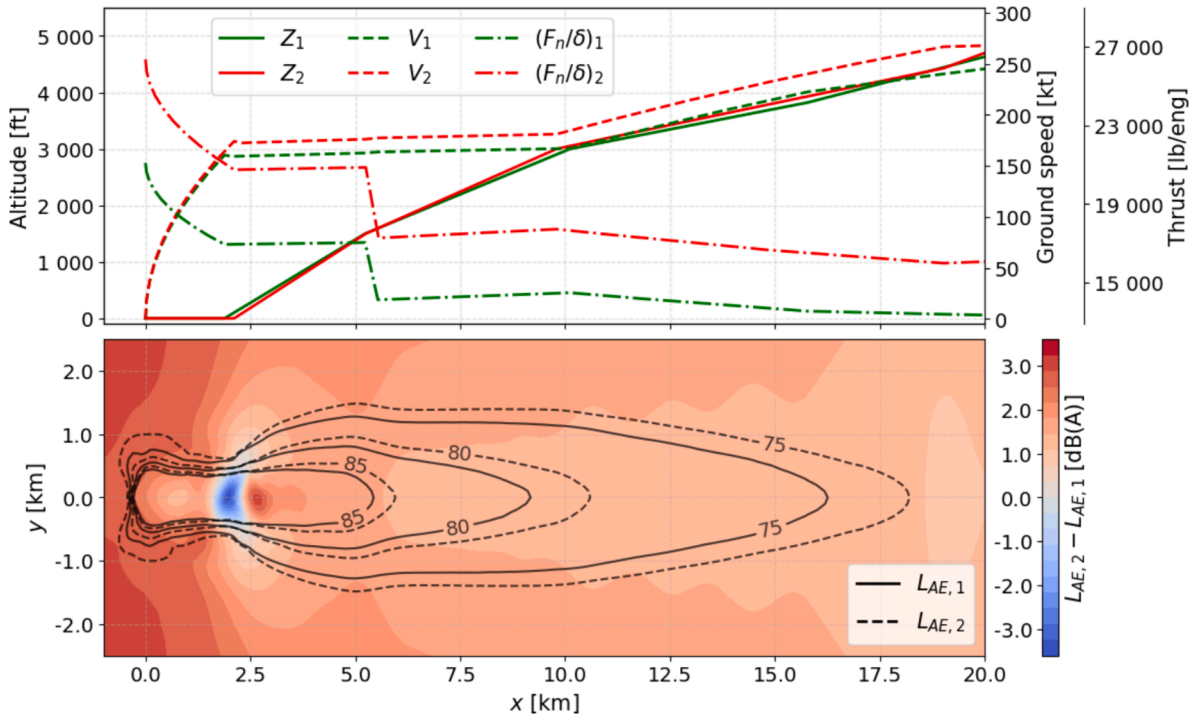

Fig. 10. (top) low-weight (1) and max-weight (2) flight profiles of a 737 MAX 8 performing an ICAO_A departure, and (bottom) impact of the weight difference with similar kinematic profiles on the L_{AE} (SEL) footprint.

higher that the low-weight case. This indicates that the inability to discern between low- and high-weight departures may lead to large noise prediction errors, and that an overall RMS_{ZV} is not enough to make this choice properly. This is why in the present work emphasis is placed on the lift-off point and the following initial climb, where both speed and altitude depend on the aircraft TOW, and the impact of external factors (e.g., wind direction change due to aircraft turns, unknown at-altitude weather, air traffic control orders) is smallest. As a result, the $K_{MTOW,est}$ estimated using Eq. (4) plays a key role in the penalty of Eq. (5), and RMS_{ZV} is weighed the highest when closest to the ground.

3.2.2. *Mixed approach applied to the arrival flight profiles*

Similarly to what done for departures, the improvements achieved with the upgraded mixed approach applied to arrivals are presented as statistical distributions involving the ratio between optimized and non-optimized RMS_{ZV}, with the latter ($RMS_{ZV,unopt}$) computed using the unaltered ANP procedures. Firstly, Fig. 11(a) shows the distribution of RMS_{ZV} ratio for all arrivals, reporting also a median of 0.22, which implies an overall improvement close to 80 %. This value is markedly higher than that of departures, and it is mostly due to the fact that landing procedures are on average more constrained than departure ones, thus allowing the ANP profiles to match better the ADS-B data. This is supported by the proxy-wise distributions in Fig. 11(b), where the median is under 0.4 even for the worst proxy. Moreover, although it is true that the proxies that refer to the most common aircraft continue to yield better results compared to the smaller ones, these differences are now much less pronounced. It would be of major interest to examine whether the resulting thrust outputs, fundamental for the noise estimation, are closer to the actual values or at least more realistic than those of the baseline ECAC method, but the lack of literature data prevents any further assessment. Therefore, the only way to obtain at least an indirect validation is the examination of noise levels and contour maps.

3.3. *Airport noise levels*

As mentioned, a major benefit in selecting Zurich Airport as a test case is that considerable attention is devoted to aircraft noise, with abundant and publicly available documentation (Flughafen Zürich, 2023). Within it are the official 2022 $L_{Aeq,day}$ contours, calculated using the FLULA2 noise computation program (Empa, 2010) fed with radar data referring to the entire year, which can be compared with the current noise predictions, obtained using a 50 km x 50 km grid of observers centred around the ARP with a 500-meter resolution in both directions and including actual terrain elevation. The calculation was conducted both without and with the mixed analysis-synthesis approach, which enabled estimating its impact on the airport noise. In both cases, $L_{Aeq,day}$ was computed as per Table 4, but cumulating all 23-day 16-hour-daytime sound energy and distributing it over this time period.

The comparison with the official contours is shown in Fig. 12(a) referring to the predictions without mixed approach, and in Fig. 12 (b) with the contours obtained including the mixed approach. Globally, both sets of predicted contours exhibit similar shapes to the official ones, suggesting that the 23-day set chosen in Section 3.1 can approximate quite well also a full-year noise calculation. However, some differences arise after more careful observation of the results. In particular, compared to the non-optimized contours, the optimized ones are noticeably longer and larger along two of the four major flight directions away from the airport, South-East and South-West, marginally longer along the other two, North-West and East, and slightly smaller near the airport (1–4 km from the ARP). This is consistent with previous outcomes (Pretto, et al., 2022), and it depends mostly on the use of $K_T = K_C = 1$ in the non-optimized departures: the use of maximum thrust leads to higher near-runway noise, but also causes the aircraft to climb more quickly, thus lowering the sound energy that reaches the ground farther from the airport. An additional contribution comes from the ICAO_A procedures, which have a longer initial climb than the default ones: this causes lower near-airport noise, but extends the footprint 1 to 2 km along the ground track (ECAC, 2016a). Finally, the impact of the optimized arrivals is mostly obscured by the averagely noisier

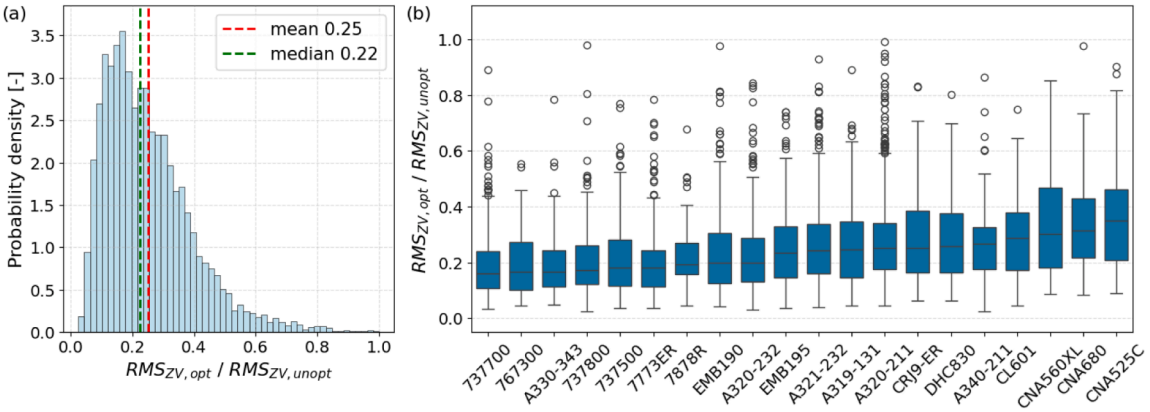

Fig. 11. (a) distribution of RMS_{ZV} ratio considering all arrivals, and (b) RMS_{ZV} ratio for each ANP proxy ordered by median, with blue bars and black lines denoting confidence intervals of 50 % and 95 %, respectively (empty circles = outliers beyond 95 % confidence). (For interpretation of the references to colour in this figure legend, the reader is referred to the web version of this article.)

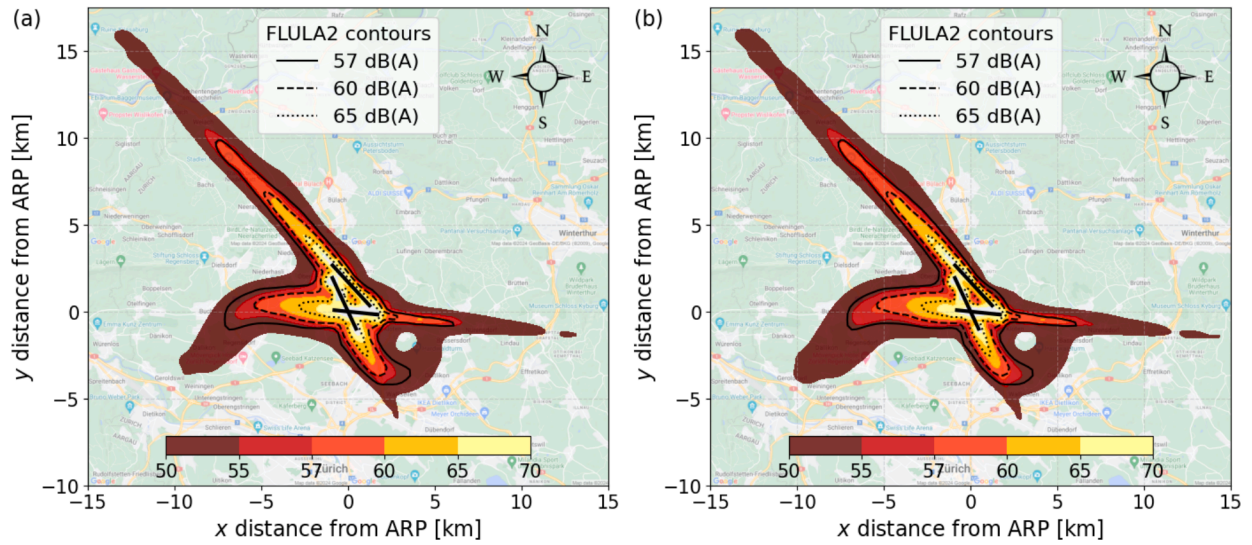

Fig. 12. Comparison between official FLULA2 and predicted $L_{Aeq.day}$ contours: (a) contours computed without profile optimization, and (b) with flight profiles optimized by applying the mixed analysis-synthesis approach.

departures, but it is slightly visible to the East of the airport along runway 10, rarely used for take-offs, and results in a longer and larger footprint that is also closer to the official contours.

Another key element highlighted by Fig. 12 is that both sets of predicted contours are smaller than the official ones, with an underestimation seemingly between 1 and 2 dB(A) depending on location and contour set. Quantification of this disagreement and of the improvement achieved with the mixed approach is paramount, but looking solely at the contour areas is misleading due to the different phenomena dominating the noise levels near the airport and far away from it. Instead, this task is best carried out using the 14 ATANOMS stations displayed in Fig. 6(b) and their noise measurements, published in monthly reports where the daily $L_{Aeq.day}$ values are provided for each station (Flughafen Zürich, 2023). Therefore, the present (non-optimized and optimized) calculation was conducted also on an array of observers located at the same coordinates as the 14 stations.

The comparison between predicted and ATANOMS results is shown in Fig. 13. Firstly, a station-wise analysis is conducted in Fig. 13 (a), which reports for each station the median and confidence interval of the differences between modelled and measured $L_{Aeq.day}$ across all the 23 days considered. Indeed, the figure confirms the qualitative observations made referring to Fig. 12. The most striking result is that in 11 out of 14 stations the noise underestimation caused by the non-optimized profiles is noticeably reduced by the mixed approach, with very clear improvements (around 1 dB(A)) for stations 6, 7, 8, 10, and 14. The only exceptions to this trend are the stations closest to the runways, stations 1, 3, and 9, where the non-optimized operations lead to equal or higher noise levels, which even exceed the measured values in stations 3 and 9. This is because the non-optimized departure profiles use maximum thrust and the default procedures, which are noisier than their ICAO_A counterparts near the runways, but these two modelling choices are inconsistent with both the literature observations and the outcomes of the optimization reported in Section 3.2.1. These considerations suggest that the mixed approach is a markedly better modelling strategy, but the initial climb phase may require some improvements, to be considered in future developments. Additionally, it is worth noting that in station 12, the farthest from the airport and affected mainly by arrivals, the median underestimation is almost 5 dB(A), with a 95 % confidence interval nearing 20 dB(A), and the mixed approach yields only a minor improvement. This outlier is mainly due to ECAC noise engine and NPD tables, which tend to underestimate the noise output at large distances (ECAC, 2016a), but roles may be played by the slightly lacking ADS-B coverage, which could have caused the loss of some arrivals, or by the arrival profile estimation, more constrained than that of departures.

Finally, to obtain an overall quantification of the improvement, any geographical information is removed and all modelled-measured $L_{Aeq.day}$ differences at the 14 stations are expressed as PDFs in Fig. 13(b) for both non-optimized and optimized (mixed approach) profiles. The figure shows that the mixed approach lowers the average noise underestimation by 0.26 dB(A), from 1.95 to 1.69 dB(A), but also that the standard deviation drops by almost 0.5 dB(A), from 2.86 to 2.37 dB(A). This result is essentially in line with those previously obtained by the authors for Heathrow and Gatwick airports, where the underestimation of exposure-based noise levels turned out to be about 1.5 to 1.6 dB(A) (Pretto, et al., 2022), and the minimal differences can be easily explained by the different airports used for the validation and by the slightly lower traffic coverage of the OSN dataset (96.7 % against nearly 99 %). Therefore, it can be concluded that the upgraded mixed analysis-synthesis approach presented in this work is capable of providing both more accurate (lower mean underestimation) and more precise (lower spread) noise predictions than the default ECAC method, the remaining error being probably caused, at least in part, by limitations of ECAC noise engine and especially NPD tables (Zaporozhets & Levchenko, 2021). Addressing such limitations goes beyond the scope of the present work, but it may constitute a promising topic of future research.

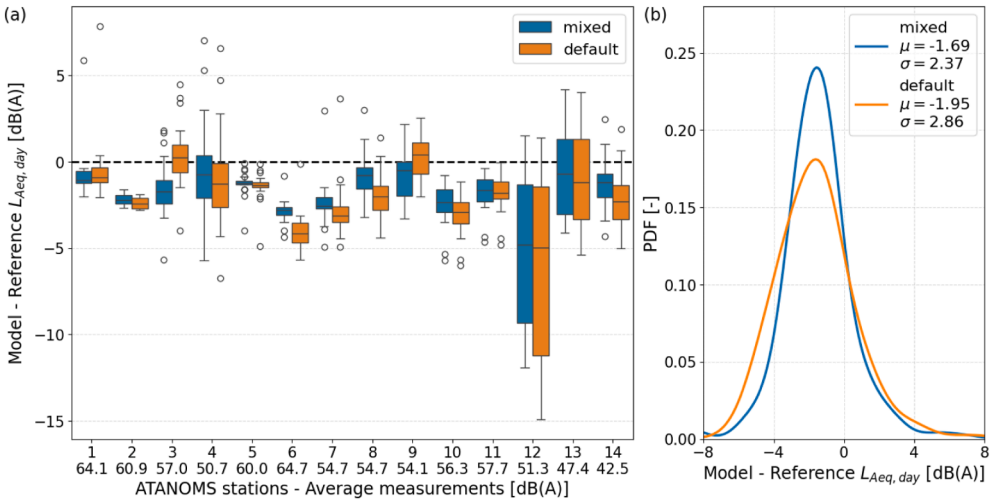

Fig. 13. (a) station-wise $L_{Aeq,day}$ differences between modelled and ATANOMS levels expressed as medians, 50 %, and 95 % confidence intervals (empty circles = outliers beyond 95 % confidence), and (b) PDFs of all $L_{Aeq,day}$ differences grouping together all 14 stations. Results are shown for $L_{Aeq,day}$ differences without mixed approach (default) and including it (mixed).

4. Conclusions and future developments

The wide and constantly increasing availability of open data on civil air traffic can be a powerful support for environmental impact assessments around airports, but only if the gap between traffic data and assessment tools, still significant, is bridged. This is the main objective of the present work, where daily aircraft operations compatible with the IMPACT/Doc 29 method were reconstructed on the basis of highly time-resolved air traffic datasets from OSN and dedicated support databases. This information was used for the identification of departures and arrivals at specific airports and for the ground track reconstruction, now more effective thanks to the high resolution and the new algorithms leveraging it. This higher resolution was accounted for also in the TMA aircraft performance (flight profile) estimation, conducted with an upgraded mixed analysis-synthesis approach that relies more heavily on the ADS-B data, no longer requiring external information on aircraft load factors. Finally, the reconstructed flight paths were used to compute airport noise levels and contour maps. The results are presented for Zurich Airport and its air traffic in 2022, where 23 days were selected to represent the entire year based on traffic coverage and weather conditions, among which key were the daily wind directions. After successfully validating the reconstructed ground tracks, analysis of the results yielded by the new mixed approach shows its effectiveness at identifying the TMA procedures, with limitations only for the departures of small aircraft. This is further confirmed by the noise predictions, which show a better estimation of airport noise levels considering contour maps and especially actual measurements at 14 monitoring stations, for an average underestimation of 1.69 dB(A).

The major merits of this work are the use of highly resolved and freely available air traffic data for reliable reconstruction of aircraft operations in the TMA, with special emphasis on the aircraft TOW estimation during departures, and the calculation of yearly average noise levels with just a small subset of representative days. However, the results obtained for both aircraft performance and airport noise suggest that the increased data density is not yet used to its full potential. An undeniable limitation is the need for adhering to the sequences of ANP procedural steps, which can be altered but that, in the end, must still be followed. This could be overcome by an increased reliance on the tracking data, which may provide more freedom in identifying the different flight segments (Sun, et al., 2017), possibly allowing to capture even non-standard procedures such as the continuous climb operations (Pérez-Castán, et al., 2018). Then, in addition to addressing the limitations of NPD tables, another improvement would be the inclusion of fuel flow and pollutant emission models, to be applied also to the taxi phases now identifiable from the on-ground ADS-B data. Moreover, extension of this tracking-based modelling tool to more airports could enable identification of statistical dispersions for both ground tracks and flight profiles, whose parameters may improve the IMPACT/Doc 29 scenario generation methods for present and future air traffic. In the longer term, the plan is to provide a reliable and effective modelling tool for the estimation of all detrimental emissions in airport areas.

5. Role of the funding sources

The authors are grateful to the European Commission for supporting this work, performed within the NEEDED project, funded by the European Climate, Infrastructure and Environment Executive Agency (Grant Agreement no. 101095754). This publication solely reflects the authors' view and neither the EU, nor the Funding Agency can be held responsible for the information it contains.

CRediT authorship contribution statement

Marco Pretto: Writing – review & editing, Writing – original draft, Validation, Software, Methodology, Investigation,

Conceptualization. **Lorenzo Dorbolò:** Writing – review & editing, Visualization, Validation, Software, Methodology, Investigation, Formal analysis, Data curation. **Pietro Giannattasio:** Writing – review & editing, Supervision, Software, Resources, Methodology, Funding acquisition. **Alessandro Zanon:** Writing – review & editing, Resources, Project administration, Funding acquisition.

Declaration of Competing Interest

The authors declare that they have no known competing financial interests or personal relationships that could have appeared to influence the work reported in this paper.

Data availability

The data are publicly available on various (referenced) sources.

References

Ansell, P.J., 2022. Hydrogen-Electric Aircraft Technologies and Integration: Enabling an environmentally sustainable aviation future. IEEE Electrif. Mag. 10 (2), 6–16.

De Gennaro, M., et al., 2018. Big data for low-carbon transport: an overview of applications for designing the future of road and aerial transport. Transport Research Arena, Vienna, p. 2018.

Degas, A., et al., 2022. A Survey on Artificial Intelligence (AI) and eXplainable AI in Air Traffic Management: Current Trends and Development with Future Research Trajectory. Appl. Sci. 12 (3), 1295.

ECAC, 2016b. Doc 29 4th Edition: Report on Standard Method of Computing Noise Contours around Civil Airport - Volume 2: Technical Guide, Neuilly-sur-Seine: ECAC.

ECAC, 2016a. *Doc 29 4th Edition: Report on Standard Method of Computing Noise Contours around Civil Airport - Volume 1: Applications Guide,* Neuilly-sur-Seine: ECAC.

Empa,, 2010. FLULA2, a Method for the Calculation and Illustration of Aircraft Noise Exposure. Technical Program Documentation (FLULA2, Ein Verfahren Zur Berechnung Und Darstellung Der Fluglärmbelastung. Technische Programm-Dokumentation. Federal Laboratories for Materials Science and Technology, Laboratory for Acoustics/Noise Control, Dübendorf, Switzerland.

EUROCONTROL - ANP, 2023. *The Aircraft Noise and Performance (ANP) Database: An international data resource for aircraft noise modellers.* [Online] Available at: https://www.aircraftnoisemodel.org/[Accessed 19 July 2023].

EUROCONTROL, 2022. *EUROCONTROL Aviation Outlook 2050.* [Online] Available at: https://www.eurocontrol.int/publication/eurocontrol-aviation-outlook-2050 [Accessed 22 November 2023].

EUROCONTROL, 2023. *EUROCONTROL Seven-Year Forecast 2023-2029.* [Online] Available at: https://www.eurocontrol.int/publication/eurocontrol-forecast-update-2023-2029[Accessed 18 December 2023].

EUROCONTROL, 2024. *IMPACT: Integrated aircraft noise and emissions modelling platform.* [Online] Available at: https://www.eurocontrol.int/platform/integrated-aircraft-noise-and-emissions-modelling-platform[Accessed 11 March 2024].

Filippone, A., 2014. Aircraft noise prediction. Prog. Aerosp. Sci. 68, 27–63.

Filippone, A., Parkes, B., Bojdo, N., Kelly, T., 2021. Prediction of aircraft engine emissions using ADS-B flight data. Aeronaut. J. 125, 988–1012.

Flughafen Zürich AG, 2023. *Aircraft noise – monitoring using measurements.* [Online] Available at: https://www.flughafen-zuerich.ch/en/company/responsibility/noise-and-sound-insulation/noise-monitoring[Accessed 11 December 2023].

Flughafen Zürich AG, 2024a. *Statistics Report 2023.* [Online] Available at: https://www.flughafen-zuerich.ch/newsroom/asset/17c40168-6b92-4acb-a04b-22d2a6b57727/statistisches-jahrbuch-2023/[Accessed 11 March 2024].

Flughafen Zürich AG, 2024b. *Flight movements – current and executed flight operations.* [Online] Available at: https://www.flughafen-zuerich.ch/en/company/responsibility/noise-and-sound-insulation/flight-movement-statistics[Accessed 26 February 2024].

IATA, 2023. *IATA Annual review 2023.* [Online] Available at: https://www.iata.org/en/publications/annual-review/[Accessed 17 November 2023].

ICAO, 2023. *Global trends in Aircraft Noise.* [Online] Available at: https://www.icao.int/environmental-protection/Pages/Noise_Trends.aspx[Accessed 18 November 2023].

Koudis, G., et al., 2017. Airport emissions reductions from reduced thrust takeoff operations. Transp. Res. Part D: Transp. Environ. 52, 15–28.

Megginson, D., 2024. *OurAirports.* [Online] Available at: https://ourairports.com[Accessed 18 March 2024].

Olive, X., 2019. Traffic, a toolbox for processing and analysing air traffic data. J. Open Source Software 4 (39), 1–3.

Pérez-Castán, J.A., et al., 2018. Impact of continuous climb operations on airport capacity. Transp. Res. Part C: Emerg. Technol. 96, 231–250.

Pretto, M., et al., 2019. Web data for computing real-world noise from civil aviation. Transp. Res. Part D: Transp. Environ. 69, 224–249.

Pretto, M., et al., 2020. Forecasts of future scenarios for airport noise based on collection and processing of web data. Eur. Transp. Res. Rev. 12 (1), 1–14.

Pretto, M., Giannattasio, P., De Gennaro, M., 2022. Mixed analysis-synthesis approach for estimating airport noise from civil air traffic. Transp. Res. Part D: Transp. Environ. 106, 103248.

Pretto, M., Dorbolò, L., Giannattasio, P., 2023. [Poster] Exploiting high-resolution ADS-B data for flight operation reconstruction towards environmental impact assessment. Journal of Open Aviation Science 1 (2).

Rekkas, C., Rees, M., 2008. Towards ADS-B implementation in Europe. In: 2008 Tyrrhenian International Workshop on Digital Communications - Enhanced Surveillance of Aircraft and Vehicles. IEEE, Capri, Italy, pp. 1–4.

Schäfer, M. et al., 2014. Bringing up OpenSky: A large-scale ADS-B sensor network for research. In: *IPSN-14 Proceedings of the 13th International Symposium on Information Processing in Sensor Networks.* Berlin, Germany: IEEE, pp. 83-94.

Schwab, O., Zellmann, C., 2020. Estimation of Flight-Phase-Specific Jet Aircraft Parameters for Noise Simulations. J. Aircr. 57 (6).

Sun, J., Ellerbroek, J., Hoekstra, J.M., 2017. Flight extraction and phase identification for large automatic dependent surveillance–broadcast datasets. Journal of Aerospace Information Systems 14 (10), 566–572.

Sun, J., Ellerbroek, J., Hoekstra, J.M., 2019. WRAP: An open-source kinematic aircraft performance model. Transportation Research Part c: Emerging Technologies 98, 118–138.

Sun, J., Hoekstra, J.M., Ellerbroek, J., 2020. OpenAP: An open-source aircraft performance model for air transportation studies and simulations. Aerospace 7 (8), 104.

Syd Ali, B., Schuster, W., Ochieng, W., Majumdar, A., 2016. Analysis of anomalies in ADS-B and its GPS data. GPS Solutions 20, 429–438.

Verbrugge, S., 2024. *Airlinerlist.com.* [Online] Available at: https://www.planelist.net/[Accessed 26 March 2024].

Wales, D.J., Doye, J.P., 1997. Global optimization by basin-hopping and the lowest energy structures of Lennard-Jones clusters containing up to 110 atoms. Chem. A Eur. J. 101 (28), 5111–5116.

Zaporozhets, O., Levchenko, L., 2021. Accuracy of noise-power-distance definition on results of single aircraft noise event calculation. Aerospace 8 (5), 121.